ISBN: 978-3-95450-241-7 ISSN: 2673-5350 doi:10.18429/JACoW-IBIC2022-TH2C2

UPGRADED CMS FAST BEAM CONDITION MONITOR FOR LHC RUN 3 ONLINE LUMINOSITY AND BEAM INDUCED BACKGROUND MEASUREMENTS

Joanna Wańczyk*,[1]
on behalf of CMS Collaboration, CERN, Geneva, Switzerland
[1]also at Swiss Federal Institute of Technology Lausanne (EPFL), Lausanne, Switzerland

Abstract

The Fast Beam Condition Monitor (BCM1F) for the CMS experiment at the LHC was upgraded for precision luminosity measurement in the demanding conditions foreseen for LHC Run 3. BCM1F has been rebuilt with new silicon diodes, produced on the CMS Phase 2 outer tracker PS silicon wafers. The mechanical structure was adapted to include a three-dimensional printed titanium circuit for active cooling of the BCM1F sensors. The assembly and qualification of the detector quadrants were followed by the integration with the Pixel Luminosity Telescope (PLT) and Beam Conditions Monitor for Losses (BCML1) on a common carbon fibre carriage. This carriage was installed inside the Compact Muon Solenoid (CMS) behind the CMS pixel detector, at a distance of 1.9 m from the interaction point (IP). BCM1F will provide a real-time luminosity measurement as well as a measurement of the beam-induced background, by exploiting the arrival time information of the hits with a sub-bunch crossing precision. Moreover, regular beam overlap scans at CMS were introduced during Run 2, enabling an independent and nondestructive transverse profile measurement for LHC Operators. These proceedings describe the improved BCM1F detector design, its commissioning, and performance during the beginning of Run 3 operation.

INTRODUCTION

The Fast Beam Condition Monitor (BCM1F) is a dedicated, standalone luminometer, independent from all central CMS services. The sub-bunch crossing (BX) precision, enables the measurement of beam-induced background. The complete detector consists of four C-shapes (see Fig. 1), with a total of 48 channels. Each C-shape pair forms a ring around the beam pipe at an approximate radius of 7 cm, on either side of the interaction point (IP). In Run 2 good performance was achieved with mixed sensor types were used (sCVD, pCVD and Silicon). The Silicon sensors had much better signal-noise separation and response linearity [1].

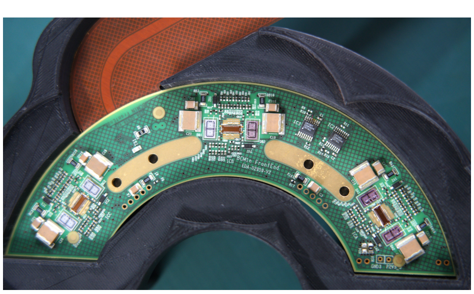

Figure 1: Picture of the Run 3 BCM1F C-shape.

* jwanczyk@cern.ch, joannawanczyk@epfl.ch

DETECTOR DESCRIPTION

The full system diagram including both the front end and the two parallel back ends is shown in Fig. 2. The detector was completely rebuilt during Long Shutdown 2 (LS2), with radiation hard sensors made of acceptor-doped (p-type) silicon. To provide high performance operation throughout Run 3 period, a three-dimensional (3D) printed titanium active cooling loop was added.

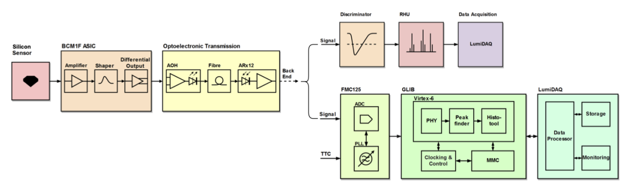

Figure 2: Diagram of the BCM1F detector architecture [2].

Front-End Electronics

Each C-shape is a single flex-rigid printed circuit board, which includes all front-end components: double silicon diodes, ASIC chips, and opto-electronic readout.

The new sensors were produced as a part of the CMS Phase 2 Outer Tracker sensor production [3]. The 300 µm thick wafers were prepared as double silicon sensors, each with dimensions of $1.7 \times 1.7\,\mathrm{mm}^2$. They are A/C-coupled to protect the amplifier from the leakage current, thus providing better signal-to-noise ratio (SNR). The signal is shaped with the fast asynchronous ASIC from the Run 2 design [4], implemented in IBM 130 nm. It provides a short peaking time (<10 ns), narrow pulses, as shown in Fig. 3, and sub-bunch timing resolution. The optical readout is placed at a larger distance from the IP, and uses analog-opto-hybrids (AOH), which convert the current into infrared light at a wavelength of 1310 nm.

The assembly and qualification of the detector quadrants were followed by integration with the Pixel Luminosity Telescope (PLT) and Beam Conditions Monitor for Losses (BCML1). Commissioning was done during the 2021 LHC pilot beam test at the injection energy of 450 GeV.

Back-End Electronics

The optical signal is converted into an 8 −bit-equivalent electric signal at the ARx12 optical receiver in the CMS service cavern (USC), shielded from the prompt radiation in the

ISBN: 978-3-95450-241-7
ISSN: 2673-5350
doi:10.18429/JACoW-IBIC2022-TH2C2

experimental cavern. Subsequently, the signal is duplicated and propagated into two back end systems:

- VME system: a leading edge discriminator module (V895) is used with fixed threshold. It generates the logical output which is connected to the Real-Time Histogramming Unit (RHU) (see upper right in Fig. 2). An orbit occupancy histogram is formed with a 6.25 ns granularity (4 bins per BX). As the counts are based on the 5 ns discriminator pulses, the system is unable to differentiate the piled up pulses, causing some inefficiency.
- µTCA based system [5]: it consists of the FPGA Mezzanine Card (FMC) digitizer with a sampling frequency of 1.2024 GHz, AC coupling of the ADC inputs, and PLL to lock on the LHC bunch clock. Peak finding and histogramming is performed on the Xilinx Virtex-6 FPGA hosted by the Gigabit Link Interface Board (GLIB) (see bottom right in Fig. 2). As in the RHU, the orbit occupancy histogram is built based on the arrival time, but with enhanced resolution of 6 bins per BX. A derivative-based peak finder algorithm was implemented allowing for resolving double hits [2].

Data are acquired by the dedicated BRIL DAQ software, independent of the central CMS DAQ.

LABORATORY TESTS

The sensors were tested at DESY, and those with the best quality were chosen for the installation. The qualification was based on I-V and C-V characteristics, sensor pad and guard ring leakage current, guard ring breakthrough voltage, full depletion voltage around −260 V, capacitance after full depletion (see Fig. 4), and coupling capacitance. The

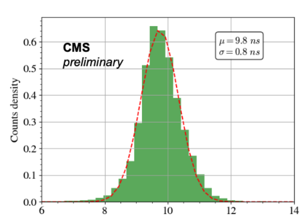

Figure 3: Distribution of the full width of radiation source pulses at half amplitude maximum.

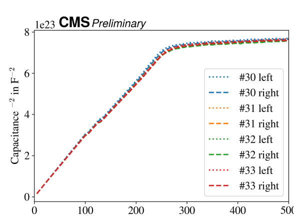

Figure 4: Sensor pad capacitance as a function of the applied high voltage bias.

C-shape PCBs were fabricated and the sensor bonding was performed at CERN. It was followed by detector-quadrant testing with internally generated test pulses as well as with a radiation source (Sr-90). The detector signal full width at half maximum (FWHM) timing distributions were in agreement with the design value: a mean around 10 ns for all channels was obtained (see Fig. 3), with the source hits amplitude spectra indicating good SNR. Prior to that, and during LS2, a test-beam was used to verify the new design with A/C coupling as well as the new cooling loop performance. The detector was finally assembled at CERN and installed in the CMS experimental cavern in July 2021.

RUN 3 COMMISSIONING

BCM1F has been operating since the beginning of LHC commissioning for the Run 3, measuring collision products at a center-of-mass energy of 13.6 TeV. During this time, the detector configuration was optimized with the per-channel timing alignment.

An example accumulated full orbit occupancy histogram is shown in Fig. 5: results from a single channel are shown using data collected over 6 hours and normalized over fixed time intervals (lumi-section, LS) of approximately 23.6 s each. In the very beginning of the orbit, occupancy corresponding to a bunch with a low occupancy signal is visible, which is caused by noncolliding bunches. It is followed by two sets of four bunch trains, which are also present later in the orbit. There are 2 individual colliding bunches present giving much narrower occupancy spikes around the bins 3000 and 10000. Afterglow tails are visible after each set of regular bunch trains, with an increased hit count observed due to the activated detector material. This signal contamination is corrected by applying an afterglow correction factor to each colliding bunch, see Fig. 6. The BCM1F uncalibrated data were fitted to an exponential function, aggregated over many orbits. The signal from the two well-separated (~µs) single colliding bunches was used, to account for the out of time hits in the following bunch crossings numbered with an identification number (BCIDs).

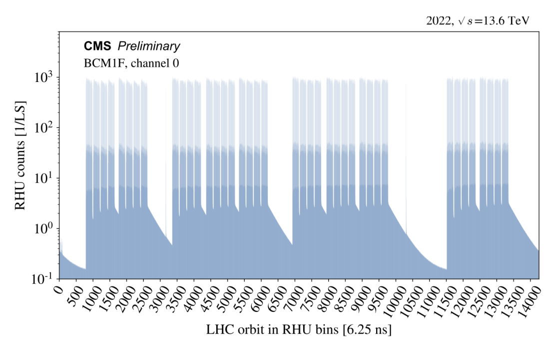

Figure 5: BCM1F measured LHC full orbit signal.

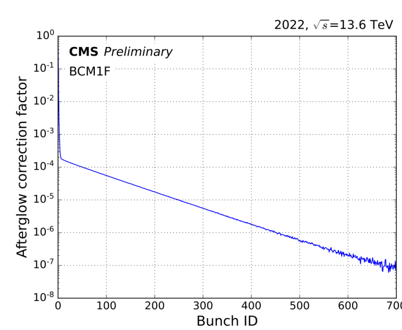

Figure 6: First Run 3 afterglow correction model based on the single colliding bunch response exponential tail.

Derivative Based Peak Finding Algorithm

The BCM1F µTCA back-end electronics was planned as an improvement to the baseline VME. The new peak finder

ISBN: 978-3-95450-241-7 ISSN: 2673-5350 doi:10.18429/JACoW-IBIC2022-TH2C2

algorithm uses a derivative based threshold, which is designed to differentiate the overlapping pulses to maintain the detection efficiency at high pileup. The derivative is calculated with a smooth noise-robust differentiator (SNRD, $N = 7$), and the peak detection is based on the derivative threshold level crossing, see Fig. 7. It was designed to provide noise suppression at high frequencies with efficient implementation into a digital system [2]. The electronics noise is also separated based on the low value of the maximum derivative, which is intrinsic to the channel performance, as well as by applying the amplitude cut off. The amplitude spectra for high energy collisions 13.6 TeV built using the new peak finder is shown in Fig. 8. The low amplitude Gaussian noise contribution was cut out with operational thresholds. The spectrum is a Landau distribution with the most probably value (MPV) corresponding to the energy loss of the minimum-ionizing particle. As the data were collected for 10 h, a higher charge deposition peaks are also observed, which correspond to the deposit of multiple MIP charges.

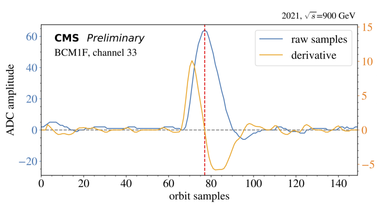

Figure 7: BCM1F µTCA sampled hit signal (blue), overlaid with the corresponding derivative (orange). The detected peak at derivative zero-crossing is marked with red line.

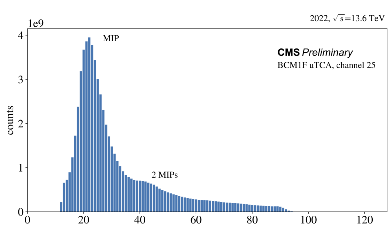

Figure 8: BCM1F µTCA per-channel amplitude spectrum.

BACKGROUND MEASUREMENT

The signals in the detector originating from beam-induced background particles are measured by different BCM1F channels, based on their location with respect to the CMS IP. Upstream beam channels are used to estimate the beam induced background. The time structure is shown in Fig. 9, where the contribution from both beams are shown at two periods within the LHC orbit. The beam direction can be defined by the time of arrival: beam 1 (B1) signal is visible in BCID 101 before beam 2 (B2), and the opposite for the second presented BCID. Based on the BCM1F measurements the beam conditions are assessed to guarantee safe operation for the other CMS subsystems. The beam-induced backgrounds measured using BCM1F are sent to the LHC as realtime feedback of the beam conditions prevalent close to the CMS experiment, see Fig. 10.

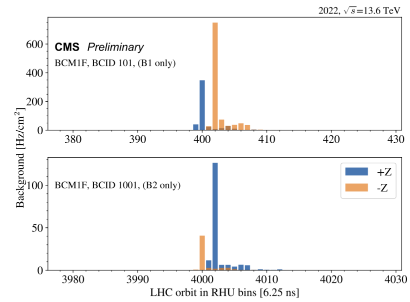

Figure 9: BCM1F average measured incoming and outgoing background for two individual nominal bunches.

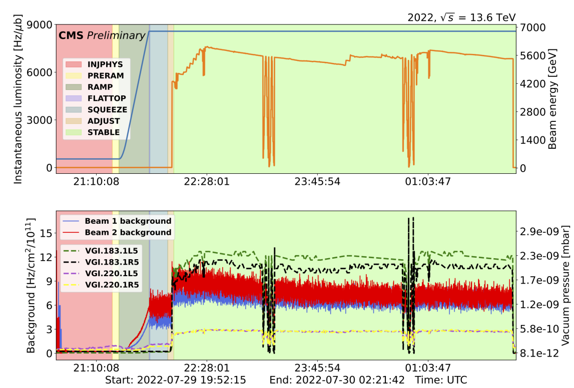

Figure 10: BCM1F measured B1 and B2 backgrounds over the LHC beam mode cycle.

LUMINOSITY MEASUREMENT

BCM1F has been the main online luminometer since the beginning of the Run 3. The luminosity measurement is based on the sum of counts within a colliding BCID. A zero counting algorithm is used, which allows for defining the average number of hits based on the zero-hit probability, and assuming that hits follow a Poissonian distribution [6].

During van der Meer (vdM) calibration [7, 8] the beam conditions are setup deliberately so that the instantaneous luminosity can be extracted from the bunch parameters, Eq. (1), using the number of colliding protons per beam $\{N_1, N_2\}$, the LHC frequency f, and the transverse convolved bunch sizes $\{\Sigma_x, \Sigma_y\}$.

$$L_{\text{inst}} = \frac{N_1 N_2 f}{2\pi \Sigma_x \Sigma_y}, \quad (1)$$

thus, the measured rate R can be used to define the visible cross section:

$$\sigma_{\text{vis}} = \frac{R}{L_{\text{inst}}}. \quad (2)$$

Subsequently, this calibration constant is used to measure the luminosity directly from the detector rate.

ISBN: 978-3-95450-241-7 ISSN: 2673-5350 doi:10.18429/JACoW-IBIC2022-TH2C2

Preliminary Calibration with Emittance Scans

As the main vdM program is planned only for the end of the year 2022, emittance scans are used to obtain preliminary detector calibration. These are short scans (10 s/step), usually performed over a narrow beam separation range (3.5 σ).

For the BCM1F µTCA each sensor is treated independently and a per channel calibration constant is extracted. The spread between good channels is within 15% from the average σ_{vis}. The stability of the online measurement can be observed with the calibration constant remeasured in subsequent scans. The BCM1F VME measurement in the early Run 3 period at nominal conditions is shown in Fig. 11, obtained as the average over all bunches per fill. The double-Gaussian fit function was used and BCM1F rate was corrected with the afterglow model and the beam induced background contribution based on the noncolliding bunch response as well as the prompt contribution just before the collision. The points were also color-coded depending on the single bunch instantaneous luminosity (SBIL). The root-mean-square (RMS) of the visible cross section in this period is 1.4%.

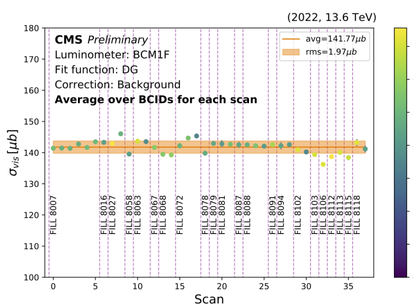

Figure 11: Calibration constant σ_{vis} over the early Run 3 period at nominal conditions.

Beam Overlap Measurement

The luminosity dependence over a separation scan includes the convolved bunch size, Eq. (1), therefore, the scans can be also used to study the bunch profile. During operation in the nominal conditions, a crossing angle ϕ is applied using the dipole corrector magnets to avoid long-range interactions. At CMS, it is applied in the horizontal plane $\{x\text{–}z\}$, hence the beam overlap includes the effect of this crossing angle:

$$\Sigma_x = \sqrt{(\sigma_{x_1}^2 + \sigma_{x_2}^2)\cos^2\frac{\phi}{2} + (\sigma_{z_1}^2 + \sigma_{z_2}^2)\sin^2\frac{\phi}{2}} \qquad \Sigma_y = \sqrt{\sigma_{y_1}^2 + \sigma_{y_2}^2}, \tag{3}$$

where σ are the bunch sizes in $\{x, y, z\}$ for B1 and B2. Figure 12 shows the bunch overlap evolution during a fill with β^* levelling in which the scans were performed after each β^* step, from 60 cm to 42 cm. The overlap width decreases along these steps.

The normalized emittance can be estimated for each plane after extracting the convolved width of the two colliding bunches σ_{eff}:

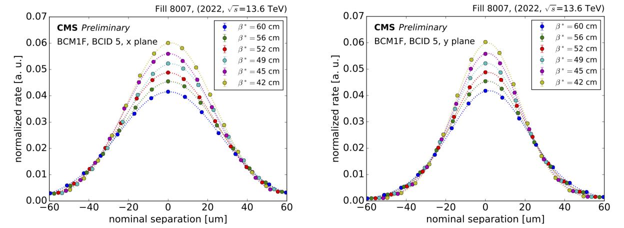

Figure 12: Evolution of beam overlap for various β^* steps during luminosity levelling. An example bunch is shown, for scans in both $\{x, y\}$ planes.

$$\epsilon = \frac{\sigma_{\mathrm{eff}}^2}{\beta^*}\gamma\beta_{\mathrm{rel}}, \qquad \sigma_{\mathrm{eff}} = \sqrt{\frac{\sigma_1^2 + \sigma_2^2}{2}}. \tag{4}$$

An example measurement is shown in Fig. 13, for a special fill which included bunches with wide range of normalized emittances: 3.95–7.25 µm in x and 1.79–5.59 µm in y.

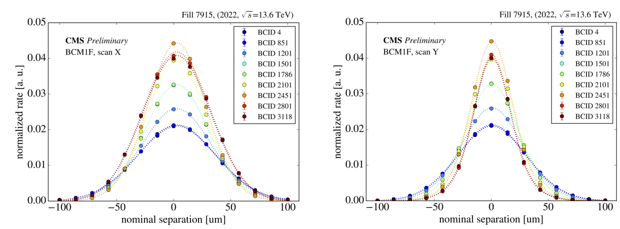

Figure 13: Beam overlap profile for 9 bunches with various emittances for both $\{x, y\}$ planes (left and right).

Orbit Displacement Measurement

The mean value is extracted from a Gaussian fit to the normalized rate over separation steps (see Figs. 12 and 13). It indicates the per-bunch orbit displacement, which is dependent on the number of parasitic collisions for a given filling pattern. An example of bunch train displacement structures measured by BCM1F for fill 8113 are shown in Fig. 14.

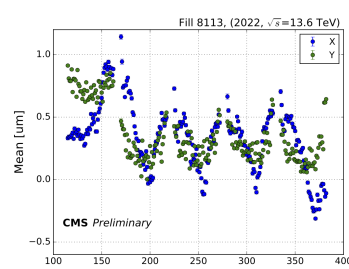

Figure 14: BCM1F measured per-bunch orbit displacement in both $\{x, y\}$ planes, zoomed into a set of bunch trains.

CONCLUSIONS

The commissioning of the upgraded BCM1F has been finalized. In the first months of the LHC Run 3, it has proven to be robust and reliable, providing CMS with online background and luminosity measurements. To achieve the best precision in luminosity, dedicated vdM calibration is necessary, planned for later in the year 2022.

ISBN: 978-3-95450-241-7 ISSN: 2673-5350 doi:10.18429/JACoW-IBIC2022-TH2C2

REFERENCES

[1] Moritz Guthoff, "The new Fast Beam Condition Monitor using poly-crystalline diamond sensors for luminosity measurement at CMS", *Nucl. Instrum. Methods Phys. Res., Sect. A*, vol. 936, pp. 717-718, 2019. doi:10.1016/j.nima.2018.11.071

[2] Alex Ruede, "New Peak Finding Algorithm for the BCM1F Detector of the CMS Experiment at CERN", Master Thesis, Ernst Abbe Hochschule Jena, 2018. https://cds.cern.ch/record/2310566/files/CERN-THESIS-2018-021.pdf

[3] Georg Auzinger, "Silicon Sensor Development for the CMS Tracker Upgrade", PhD thesis, Vienna University of Technology, 2013. https:/cds.cern.ch/record/1631093/files/CERN-THESIS-2013-211.pdf

[4] Jan Kaplon, Dominik Przyborowski, and Piotr Rymaszewski, "Design and Performance of the BCM1F Front End ASIC for the Beam Condition Monitoring System at the CMS Experiment", *IEEE Trans. Nucl. Sci.*, vol. 63, no. 4, Aug 2016. doi:10.1109/TNS.2016.2575781

[5] A. A. Zagozdzinska *et al.*, "Architecture of the upgraded BCM1F Backend Electronics for Beam Conditions and Luminosity measurement - hardware and firmware", *J. Instrum.*, vol. 10, p. C02020, 2015. doi:10.1088/1748-0221/10/02/c02020

[6] Olena Karacheban, "Luminosity measurement at CMS", PhD thesis, Brandenburg University of Technology Cottbus-Senftenberg, 2016. https://bib-pubdb1.desy.de/record/393347/files/Thesis.pdf&usg=AOvVaw3F8oI6Y0Vju1hd0XvaBUyM

[7] S. van der Meer, "Calibration of the effective beam height in the ISR", Technical Report CERN-ISR-PO-68-31, 1968. http://cds.cern.ch/record/296752/files/196800064.pdf

[8] CMS Collaboration, "Precision luminosity measurement in proton-proton collisions at $\sqrt{s}$ = 13 TeV in 2015 and 2016 at CMS", *Eur. Phys. J. C.*, vol. 81, p. 800, 2021. doi:10.1140/epjc/s10052-021-09538-2